The Synchronous Instability of a Compressor Rotor Due to Bearing Journal Differential Heating

F. M. de Jongh
Research and Development,
Demag Delaval Turbomachinery,
Delaval Stork V.o.f.,
Hengelo, The Netherlands

P. G. Morton
Consulting Mechanical Engineer,
Wolverhampton, United Kingdom

The paper describes a synchronous vibration instability problem encountered on a centrifugal compressor with oil-lubricated bearings. The problem was solved by modification of the compressor rotor; however, the root cause was not completely understood at that time. A possible explanation was based on a theory that suggested differential heating of the bearing journals. It was decided to verify this theory by experiments. Therefore a test rotor was designed with identical rotor dynamic characteristics to those of the compressor rotor. To fill a gap in the published research on bearing thermohydrodynamics, an experimental technique was devised to measure the surface temperature variations around one of the journals of this rotor. The dependence of significant temperature differentials across the journal upon its orbit was confirmed.

Introduction

Turbomachinery for offshore applications is extensively tested before it is shipped to the site. Compressor testing for these applications usually involves aerodynamic performance measurements according to the ASME/PTC-10 code [1] and API-617 mechanical running tests [2]. The subject of this paper is a vibration problem encountered during the mechanical running test on a LP/IP centrifugal compressor, for an offshore gas-lift application. The rotor of this drive-through compressor weighs around 450 kg and is supported by two oil-lubricated tilting pad bearings, each bearing having five pads arranged in a load-on-pad configuration. A longitudinal section of the compressor is shown in Fig. 1. During testing in the manufacturer's workshop, the rated speed could not be attained due to high rotor vibration.

Problem Description

After the aerodynamic performance test at reduced speed according PTC-10/Class III, the compressor was subjected to a no-load API mechanical running test. The machine was run as a stand-alone unit driven by a shop motor and gear. When the compressor was run up in speed it was impossible to achieve the rated maximum continuous speed of 11,947 rpm, because of high synchronous vibration levels of the rotor, although the casing vibration levels remained low. Figure 2 gives an example of the variation of vibration level and phase as a function of running speed, measured adjacent to the non-drive end (NDE) bearing. At speeds below 9000 rpm the shaft vibration level was low. From 9000 rpm the rotor speed was gradually increased in steps of 500 rpm up to 11,000 rpm. At this speed neither the vibration level nor the phase stabilized, but fluctuated over a certain range. A further speed increase to 11,400 rpm resulted in continuously fast growing shaft vibrations; at a level of around 50 percent of the bearing clearance the run was interrupted by reducing the speed to 10,000 rpm. After a dwell of about three minutes at this speed the vibrations returned to their original run-up values. Additional vibration measurements showed that the high vibration levels were associated with a second bending mode, i.e., a mode with three nodes, two of which were located near the bearings.

The complete rotor was rebalanced in the manufacturer's high-speed balancing facility. Although it proved to be very sensitive to small unbalances, it was found possible to run up to 13,142 rpm (10 percent overspeed) without any problems. On refitting in the compressor, however, the original unstable behavior was reproduced exactly. The rotor of a duplicate machine was then built into the compressor with identical results. Moreover, the instability persisted when, in a further run, the mechanical oil seals were removed. Also, testing showed that by reducing the NDE overhang weight, the speed at which instability occurred was increased. By removing the half coupling spacer weight as well as the coupling hub (total 13.7 kg), it was possible to achieve 10 percent overspeed. Further experimentation resulted in a final overhang weight reduction of 12.5 kg at the DE and 8.1 kg at the NDE, obtained mainly by a lighter coupling hub and by a change of coupling spacer material from steel to titanium. With this configuration a successful API rotor sensitivity test was carried out. Since additional investigation and testing on the compressor were not possible due to practical delivery time constraints, the compressor unit was shipped. No further vibration problems have recurred since commissioning at site.

It was decided that a full explanation of the unstable synchronous vibrations was required for two reasons: first, to establish the margin of safety of the machine in service, and second, to enable design rules to be formulated so that this particular problem could be avoided in the future.

Diagnosis/Theory

Whenever unstable vibrations occurred, they could be suppressed by reducing the rotor speed to 10,000 rpm. "Hysteresis" occurred, in that after reducing the speed, it took some time before the original status was restored. This ruled out the simplest explanation, namely that the machine was merely running too near to a low damped critical speed. Rotor response calculations showed a critical speed at 14,500 rpm (second bending mode), which according to the API [2] was far enough separated from the operating speed. In any case, the fact that

Contributed by the International Gas Turbine Institute and presented at the 39th International Gas Turbine and Aeroengine Congress and Exposition, The Hague, The Netherlands, June 13–16, 1994. Manuscript received by the International Gas Turbine Institute February 4, 1994. Paper No. 94-GT-35. Associate Technical Editor: E. M. Greitzer.

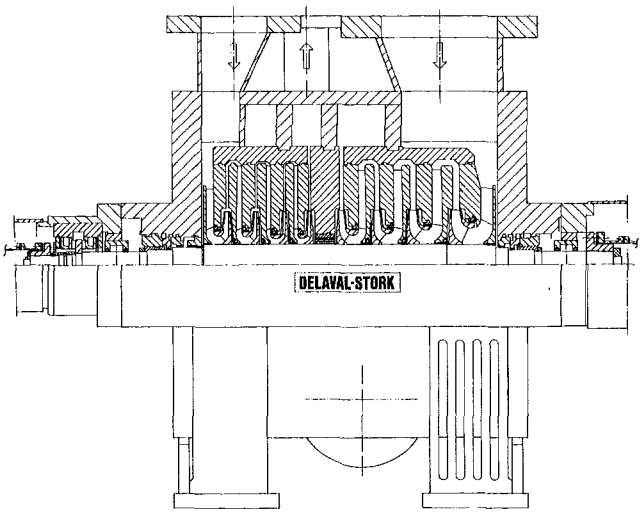

Fig. 1 Longitudinal section of LP/IP centrifugal compressor

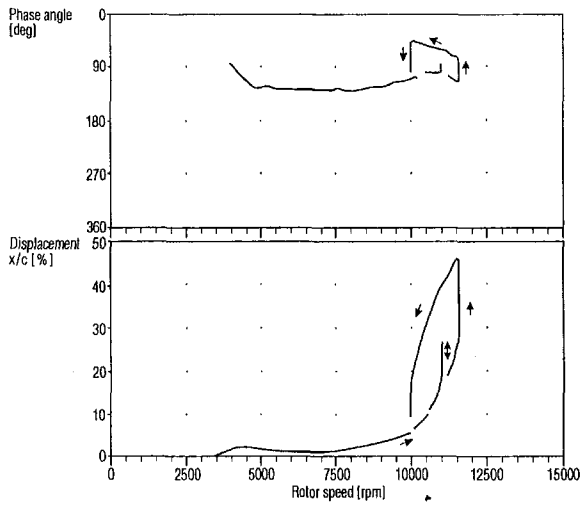

Fig. 2 Fundamental component (1X) of relative shaft vibration, measured at the N.D.E. bearing (LP/IP compressor)

the vibration level was increasing at constant speed suggested instability rather than response to unbalance. The time constants of both the growth and decay of vibrations were those normally associated with a thermal phenomenon. The indications were similar in fact to those of a seal rub in which the thermal "Newkirk effect" causes synchronous vibrations to increase, until the rotor is damaged or the rub clears due to seal abrasion [3, 4]. However, the fact that the rotor also exhibited instability with the mechanical seals and labyrinths removed precluded this rubbing possibility.

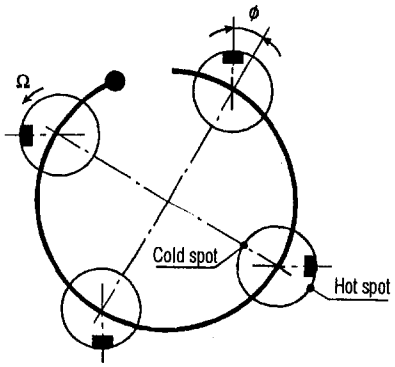

Fig. 3 Differential heating at bearing journal for synchronous forward rotor whirl

The Newkirk effect results from the contact of a stationary element with the rotor, producing a hot spot on the rotor, which in time develops a thermal bend. Any journal orbiting in a bearing can also produce a temperature difference across a diameter due to differential shearing in the oil-film. This causes the rotor to bend. It has been shown that this thermal bend, if powerful enough, in conjunction with dynamic amplification due to running in the vicinity of a critical speed, can under certain circumstances generate unstable vibrations [5–7].

Explanation of Mechanism

Since no rotor is perfectly balanced, every journal will always execute some orbit within the bearing. The orbit will in general be an ellipse whose center is eccentric to the geometric center of the bearing. In a linear system the elliptical orbit can be decomposed into a forward and a backward circular orbit, thus:

$$x = X \cos(\Omega t + \alpha) = \frac{X}{2}\{e^{i(\Omega t+\alpha)} + e^{-i(\Omega t+\alpha)}\} \quad (1)$$

$$iy = iY \sin(\Omega t + \beta) = \frac{Y}{2}\{e^{i(\Omega t+\beta)} - e^{-i(\Omega t+\beta)}\} \quad (2)$$

whence:

$$x + iy = \left(\frac{Xe^{i\alpha} + Ye^{i\beta}}{2}\right) e^{i\Omega t} + \left(\frac{Xe^{-i\alpha} - Ye^{-i\beta}}{2}\right) e^{-i\Omega t} \quad (3)$$

Considering first the forward orbit, it can be seen from Fig. 3 that in the case of synchronous vibration, one point on the journal will always be nearest to the bearing wall and the point opposite, farthest from it. A study of the thermohydrodynamics of the bearing is a complex matter, but it can be stated that the heat input to the journal comprises a circumferentially constant value and a sinusoidal term distributed around the rotor.

Apart from oil-film convection, there will be conduction along the rotor from the mean heat input and across the journal

Nomenclature

G = gain factor
I = influence coefficient
M_c = concentrated overhang mass
T = thermal gain
c = bearing clearance
i = imaginary unit
l = overhang length
m = mass
q = orbit vector
t = time
x, y = displacement
z = distance
α = phase angle
β = phase angle
γ = shaft slope compressor rotor
ζ = angle between the hot spot and the point of thinnest oil film on the journal
η = shaft slope test rotor
θ = change in slope at bearing location
ϕ = angle between unbalance vector and rotor displacement vector
Ω = rotational speed

Subscripts

B = bearing position
i = input
O = overhang position
o = output

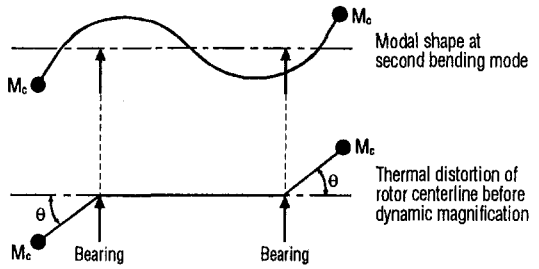

Fig. 4 Comparison of thermal bend and second bending mode

from the differential input. The latter produces a temperature differential locally across the journal, which results in a bend. Similar arguments apply to the backward whirl case when the journal is eccentric, although the heat input will always be smaller. Since linearity is assumed, the forward and backward whirl effects can be superimposed.

For the purpose of illustration, further argument will be restricted to the forward circular whirl case. Referring to Fig. 4, the thermal distortion of the rotor when stationary is shown to affect only the overhangs. Imagine for simplicity that the overhang mass is concentrated at the ends and the thermal bend θ localized at the bearings. Also consider θ arising thermally from an orbit at the bearing, denoted by vector q, then:

$$\theta = T(t, \Omega)q \tag{4}$$

where θ defines both magnitude and direction relative to rotor axes. T is a complex number varying with time and speed. Consider now a small bend θ_i imposed on this rotor at the bearing location. This results in an unbalance at the overhang of $M_c l\theta_i$. According to the influence coefficient balancing theory [8], the orbit produced at the bearing will be:

$$q = M_c l\theta_i I_{OB} \tag{5}$$

where I_{OB} is the influence coefficient between the overhang and bearing locations. Applying q to the bearing, then from Eq. (4) the value of θ resulting from thermal action will be:

$$\theta_o = TM_c l\theta_i I_{OB} \tag{6}$$

According to the control theory [9] the simple control loop of Fig. 5 is obtained, where the open loop gain is given by:

$$G = \theta_o/\theta_i = M_c l I_{OB} T \tag{7}$$

I_{OB} can be expressed as a complex number implicitly dependent on speed, mode shape, system damping, and proximity to a critical speed. A high value indicates a sensitive dynamic system. T, which is time dependent due to its thermal nature, can also be expressed as a complex number in the steady-state open-loop case, i.e., after a time elapse associated with the thermal inertia of the journal. The full theory for the time-dependent solutions is quite complex [9] but a great deal of information about stability can be found from the simple steady-state representation.

Given information either from theory or test, the values of I_{OB} and T can be obtained at any given running speed and G can be evaluated. In most practical systems there will be at least one running speed at which G becomes a real number. If this number is greater than unity, the system is unstable at that speed. If G has a negative real part, then clearly the criterion for instability is not satisfied. T will be largely negative since the orbit vector q will produce a bend whose direction results in an unbalance vector on the overhang roughly antiphase to q. The sign of the real part of G is thus strongly influenced by the sign of the real part of I_{OB}. When the latter value becomes positive, the system must be stable.

Experimental Verification

To verify the foregoing theory, it was decided to build a special test rotor, equipped with temperature sensors in one of the bearing journals in order to measure a possible temperature difference across the journal.

Design of Test Rotor. The test rotor was required to run on rotor supports, provided by an existing R&D test compressor, which would accommodate a test rotor with a bearing span of only 1041 mm instead of the original span of 1700 mm. The drive system, that is the electric motor, step-up gear and the necessary oil system, was also available. The problem then was to design a shorter test rotor with dynamic characteristics identical in all respects to the full-size machine rotor and using the same bearings.

The initial modeling proces is described in detail in the appendix, but basically the diameter of the rotor was reduced to counter the stiffening arising from shortening all rotor elements. The impellers and other additional rotor weights were simulated by simple disks. In order to maintain the same mass matrix, these disks were increased and additional disks were added. Bearings of size identical to the originals were retained. Although this process gave a dynamically identical system, the shortened overhang gave an incorrect response to the thermal bending. The overhang length of the model rotor was therefore increased and the change in dynamics was compensated for by increasing the overall stiffness of the rotor, while retaining the same mass distribution. In this way, a model for the test rotor that gave the correct influence coefficients between journal bend and journal response over the appropriate speed range was obtained. Figure 6 shows the design of the test rotor and the original compressor rotor and Fig. 7 gives a comparison of the critical speeds of both rotors. Figure 8 gives the most relevant comparison concerning the rotor response at the NDE journal for a 100 grmm unbalance at the NDE overhang. To be strictly accurate the correct response value would be that which arises from distributed unbalance of $m \cdot z$, where $m(z)$ is the incremental mass on the overhang at a distance z from the bearing. The error in concentrating the overhang mass at the coupling position is not great, however.

Journal Temperature Measurement. For verification of the theory, measurement of journal differential temperature was essential. Since the mass overhang moment at the NDE was greater than at the DE and because of the better accessibility, it was decided to measure at the NDE journal only. To develop the measuring system, preliminary experiments were conducted on a simple shaft running in the balancing facility. From these experiments small Pt-100 resistance temperature detectors (RTDs) were selected for the test rotor. Assuming that according to the theory the temperature distribution around the journal varied sinusoidally, a minimum of four sensors was required to establish the direction and magnitude of any differential temperature in the journal (Fig. 9). It was important to make as little change as possible to the heat conduction paths in the journal, so that the number and size of the sensors, as well as the guide holes for the wiring, had to be kept to a minimum. The temperature sensors were first glued into a small insert and then the assembly was mounted both with glue and

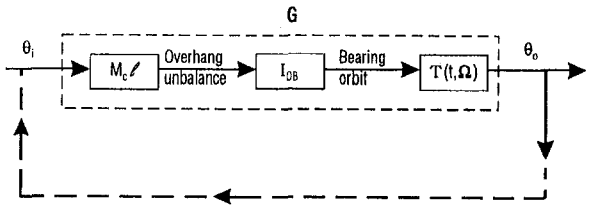

Fig. 5 Scheme of instability phenomenon

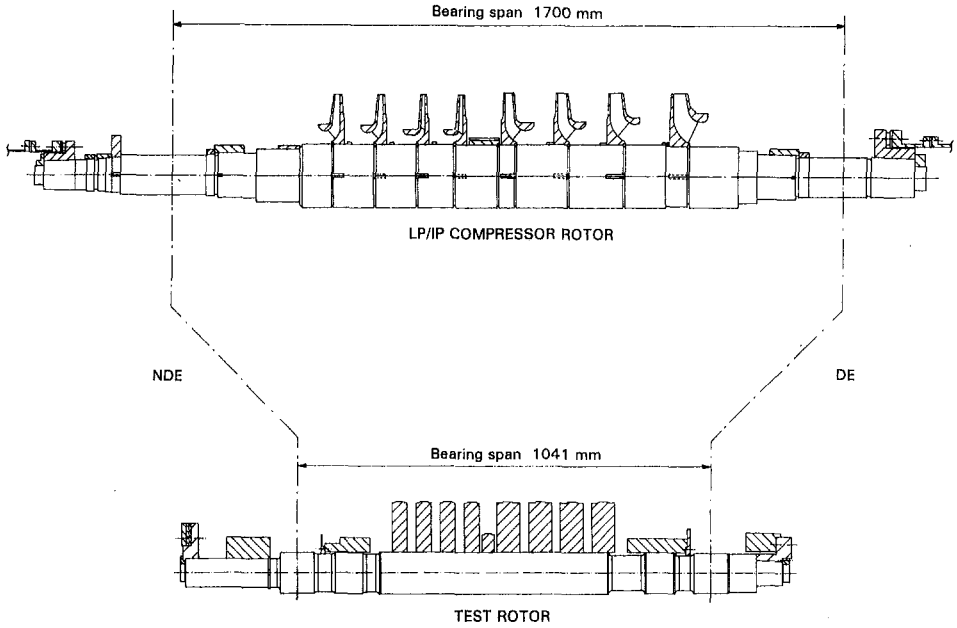

Fig. 6 Comparison of LP/IP compressor rotor and test rotor

a light interference fit into the journal, the latter to ensure a good thermal contact between sensor and journal. The sensing tip of each temperature sensor was located 1.3 mm below the journal surface. All sensors were electrically insulated from the shaft. To transfer the electrical signals from the rotating shaft to stationary measuring equipment, a special slipringless transmitter has been used. This instrument was mechanically connected to the shaft at the NDE with a flexible coupling. The temperature sensors were electrically wired to the transmitter to establish both absolute and differential temperature of the journal.

Test Setup. After the complete test rotor had been balanced at operating speed, it was built into the R&D test compressor (Fig. 10). A simple oil-lubricated axial bearing was fitted to keep the rotor in position. Since the rotor would run under atmospheric conditions, air was purged through the suction nozzle of the compressor to remove heat generated by the disk friction of the rotor. To prevent any drain oil from the bearings entering the compressor casing, labyrinth seals with an air purge were installed. The rotor was driven through a test stand planetary gear by a speed-controlled electric motor.

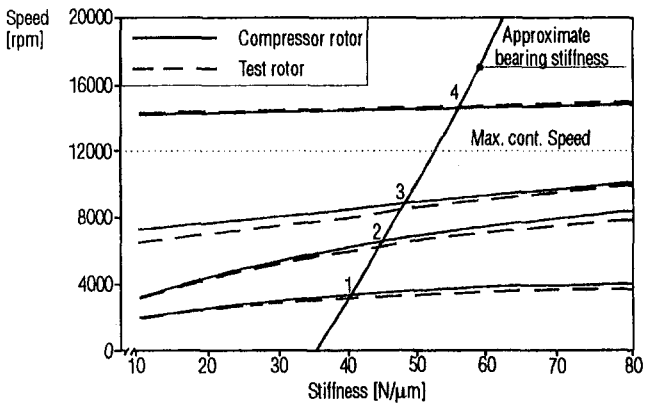

Fig. 7 Undamped critical speed map of compressor rotor and test rotor

Instrumentation. Radial shaft vibration relative to the casing was measured with noncontacting eddy-current displacement probes placed at six different locations along the test rotor, each location containing two probes spaced 90 deg apart. To correlate the journal differential temperature with the orbit size in the bearing, three additional vibration probes of the same type were mounted at the center of the NDE bearing between the pads and as a result had to be spaced 72 deg. Due to the nonorthogonality, corrections were made to obtain the correct orbit representation at this location.

Piezo-electric accelerometers were attached to the bearing pedestals both in horizontal and vertical directions to measure absolute casing vibration. A once-per-turn pulse signal was generated for phase reference and rotor speed indication. Vibration signals could be connected to oscilloscopes for time and orbit

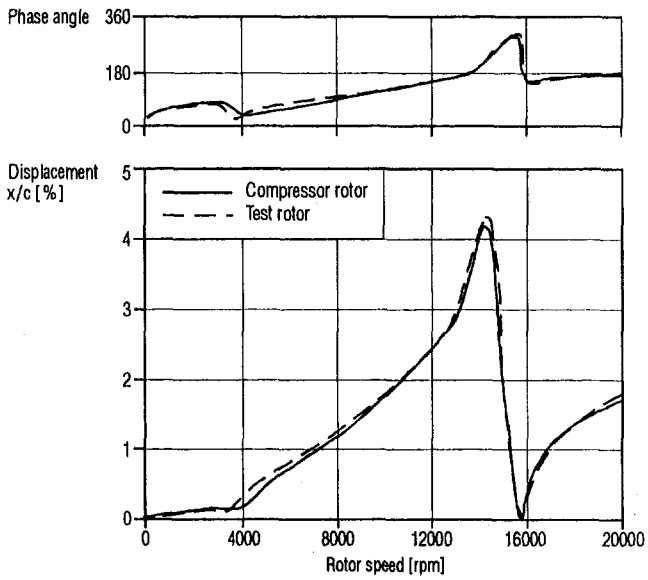

Fig. 8 Rotor response computed at the center of the N.D.E. bearing due to 100 grmm unbalance at the N.D.E. overhang

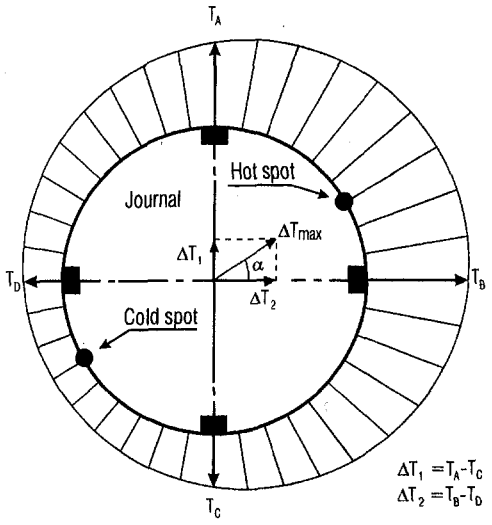

Fig. 9 Cross section of bearing journal with sinusoidal temperature distribution. Direction and magnitude of maximum temperature difference derived from four sensors.

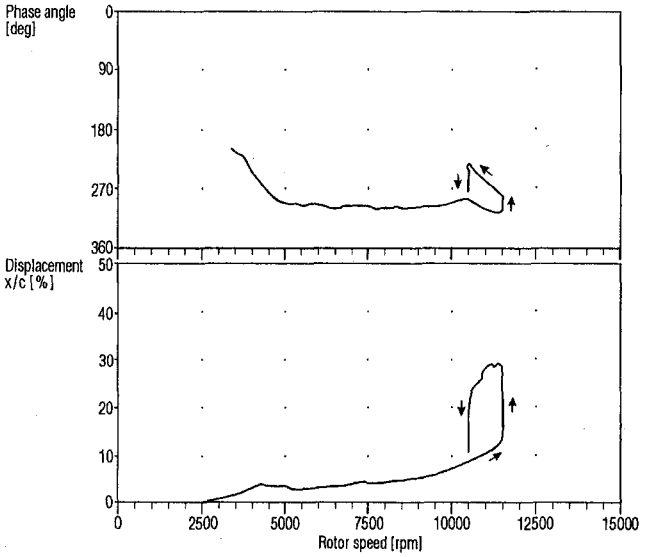

Fig. 11 Fundamental component (1*X*) of relative shaft vibration, measured at the N.D.E. bearing (test rotor)

presentation and to a two-channel FFT analyzer for frequency spectra of the individual time signals. All vibration signals were connected to an automated data acquisition system for the reduction of dynamic vibration data.

The most heavily loaded pads of the bearings were provided with temperature sensors. Thermocouples were used to measure the oil supply and drain temperatures. An orifice flow measuring device was inserted in the oil supply piping to the journal bearings.

Bearing journal differential temperatures were measured with a two-channel carrier amplifier, each channel being connected to two RTDs, which were spaced 180 deg, in a half-bridge configuration.

The vibration signals and the two journal differential temperatures were recorded on a digital tape recorder for later analysis. All other parameters were measured with an automatic data acquisition system and recorded on disk. A control monitor was capable of generating machine alarms and trips when relative shaft vibrations or bearing pad temperatures exceeded predefined set-points.

Results

Under specified bearing operating conditions, the test rotor was gradually increased in speed up to 10,500 rpm (Fig. 11). At this speed the vibration level was around 8 percent of the bearing clearance with an observed temperature difference across the bearing journal of about 3°C (Fig. 12(*a*)), but the rotor-bearing system was completely stable. When the rotor was accelerated up to 11,500 rpm, the system became unstable. Vibration was increasing at constant speed with a growth rate of about 15 percent of the bearing clearance per minute. A phase decrease was also observed. The vibration vector was spiraling in the same direction as the running speed. The differential temperatures measured at the NDE journal were continuously growing. When the vibration level reached about 30 percent of the bearing clearance, the rotor speed was reduced to 10,500 rpm and held constant. After around two minutes, the initial conditions with respect to vibration amplitude, phase,

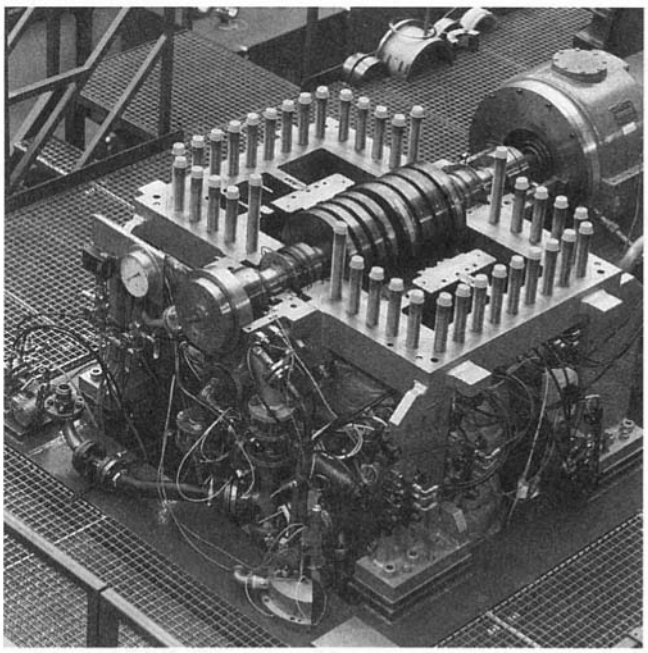

Fig. 10 Test rotor in R&D test compressor

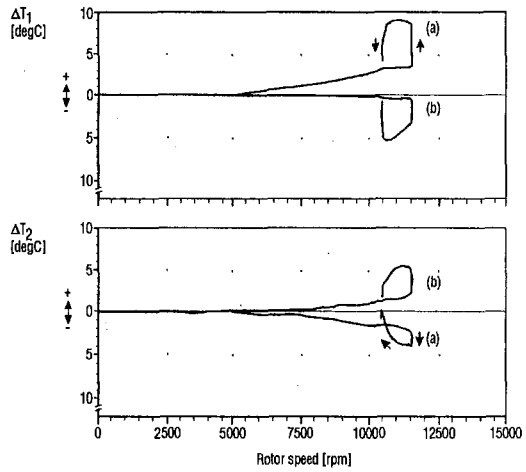

Fig. 12 Measured temperature difference at N.D.E. bearing journal: (*a*) unbalance weight at the N.D.E. overhang; (*b*) unbalance weight rotated over 180 deg

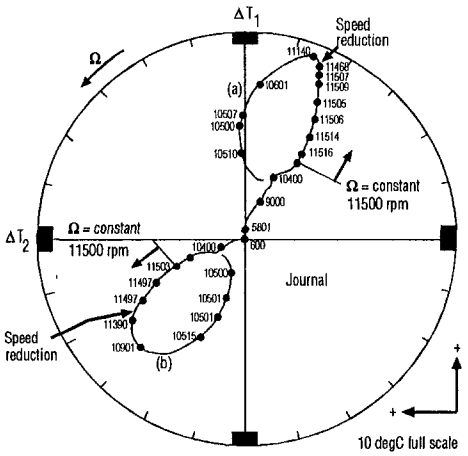

Fig. 13 Direction and magnitude of maximum temperature difference versus rotor speed: (*a*) unbalance weight at the N.D.E. overhang; (*b*) unbalance weight rotated over 180 deg

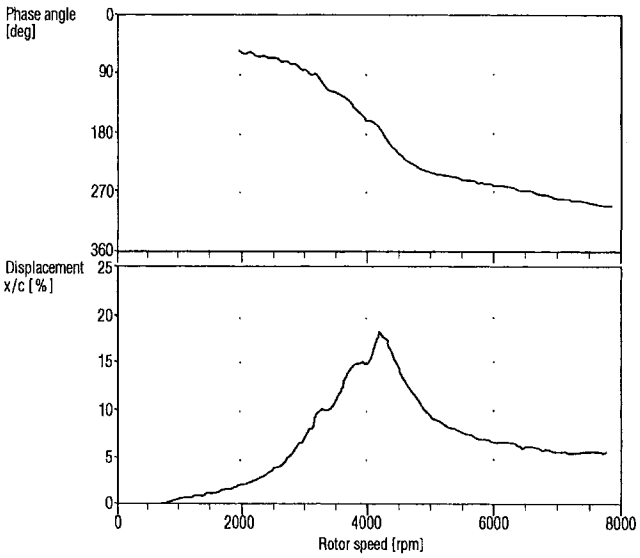

Fig. 14 Rotor response (1*X*) due to unbalance weight at midspan (passing first critical speed)

and journal differential temperature were reached again. In an attempt to establish the instability boundary more precisely, the rotor was run at 11,200 rpm. At this speed the vibration level and phase fluctuated over a range. The rotor mode shape throughout this exercise was that of the second bending mode, with large overhang deflections.

The magnitude and direction of the maximum journal differential temperature (hot spot) are shown in Fig. 13(*a*), and have been derived from the two measured differential temperatures (Fig. 12(*a*)).

The above-mentioned rotor behavior was obtained on a balanced test rotor to which a small unbalance weight was attached at the NDE overhang. This was done to force a defined point on the NDE journal circumference to be at the outside of the orbit, being the point of the thinnest oil film and so influencing the location of the hot spot. Similar results, however, were obtained without an additional unbalance weight, where the location of the hot spot was determined by the position of the residual unbalance of the rotor. Rotating the attached unbalance weight over an angle of 180 deg resulted in a change of the location of the hot spot of about the same angle (Figs. 12(*b*) and 13(*b*)). At 11,500 rpm the experiments showed a significant journal differential temperature proportional to the size of the orbit.

The journal orbit was very nearly circular and the vibration measurements showed that the journal was moving predominantly in forward whirl. The point on the journal circumference exhibiting the thinnest oil film therefore coincided with the high spot of the journal, measured with vibration probes at the center of the bearing. It was found that a phase lag existed between the point of the thinnest oil film and the hot spot on the journal circumference. At a speed of 10,500 rpm the hot spot is lagging the point of the thinnest oil film by an angle ζ of about 20 deg.

By quickly raising the rotor speed, it was found possible to run through the unstable range and reach stability at 13,600 rpm. It was thus established that the band of instability lay within the range 10,500 rpm to 13,600 rpm. The precise location of instability boundaries was clearly an impossible task because by definition the vibration growth at these speeds is around zero. Also slight variations in system parameters resulted in fluctuations in the vibration level. Somewhere in this range the rate of unstable vibration growth was at a maximum and roughly at this same region the spiraling of the journal vibration vector changed from the same direction as the rotation to the opposite direction. For reasons of safety it was judged inadvisable to dwell too long in this region, so that the exact speed of change-over in spiraling was not established.

Differential heating could also be generated by the oil seal retaining rings, which were situated on both sides of each bearing. These rings slide in grooves and should float radially to follow the rotor displacement. In the event of these rings sticking, differential journal temperatures could be generated. A test was repeated without the rings and similar results were obtained. It was concluded that the seals were functioning properly and were not contributing to the instability problem.

An additional test was carried out to observe the journal temperature behavior at lower rotor speeds. A distinct orbit could be generated at the bearing location when passing the first critical speed (4250 rpm). An excitation unbalance weight was attached at midspan of the test rotor, being the antinode of the first mode shape. A Bode plot of the run-up is shown in Fig. 14 and the measured differential temperatures are given in Fig. 15. The rotor was accelerated in speed slowly with a rate of around 150 rpm/min. When passing the critical speed, the location of the hot spot was changing continuously in one direction as a function of the phase shift between the unbalance vector and the rotor displacement vector (Fig. 16). Although additional unbalance was created due to the thermal effect, the rotor system was completely stable since in this case the open-loop gain G is smaller than unity. The measured journal differ-

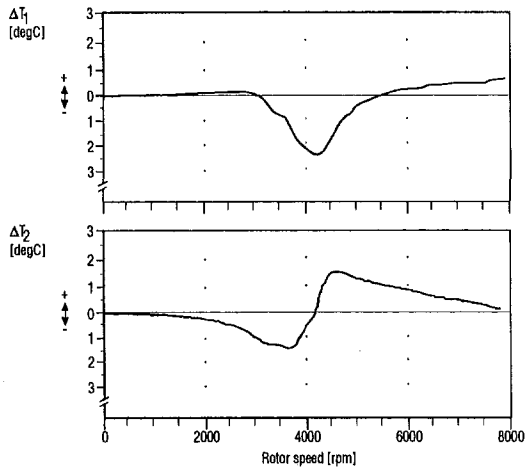

Fig. 15 Measured temperature difference at N.D.E. bearing journal (passing first critical speed)

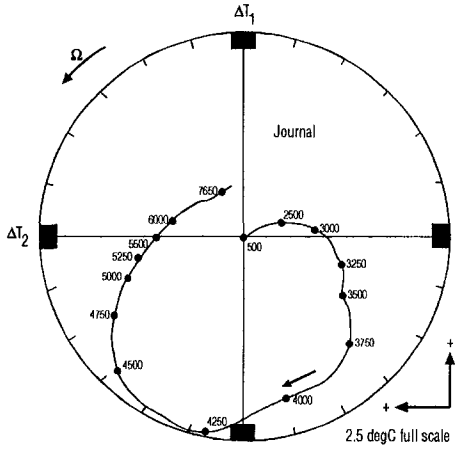

Fig. 16 Direction and magnitude of maximum temperature difference versus rotor speed (passing first critical speed)

ential temperature at a speed of 4000 rpm was about one third of that observed at 11,500 rpm. At this speed the hot spot was lagging the point of the thinnest oil film by an angle ζ of about 15 deg.

Finally, it was decided to investigate the effect on the onset of instability, of changing the overhang mass. With regard to the difficulties mentioned earlier regarding the precise location of instability boundaries, it appeared that the range was shifted upward by around 700 and 1800 rpm by reductions in the NDE coupling mass of 2 kg and 5 kg, respectively. Increases of 2 kg and 5 kg reduced the range by 800 rpm and 1300 rpm, respectively.

Discussion

At the outset, it is necessary to establish whether the test rotor correctly represented the original compressor rotor in all essential aspects. Although the test rotor was not physically identical, computed comparisons with the original machine of essential dynamic characteristics were remarkably close in the following respects:

- The critical speeds, particularly the most relevant second bending mode, were close over a wide support stiffness range.
- The response of the test rotor at the NDE journal to unbalance at the NDE overhang was very similar to that of the original compressor rotor.

Furthermore, the bearings, usually the most indeterminate components in any rotating system, were identical in terms of geometry, loading, and operating conditions.

It could be argued that the diagnosis put forward earlier in this paper would be correct, provided the same pattern of synchronous instability as in the production machine was reproduced during the test rotor experiments. In this respect the agreement was good. Although it was impossible to establish exactly the onset speed of instability, both systems were in a transitional stage at around 11,000 rpm. Also both systems exhibited very similar hysteresis effect at this boundary.

A reduction in coupling masses both at DE and NDE locations had been shown to eliminate instability within the running range on the production compressor. The experiments on the test rotor involved changing the coupling mass at the NDE only. It was clearly confirmed that such changes had a powerful effect on the onset of instability. A reduction of 5 kg in the test rotor coupling mass (around 60 percent of the reduction in the production machine), raised the onset speed to 13,000 rpm, which is roughly the 10 percent overspeed level in service. A similar increase in coupling mass reduced the onset speed to 9900 rpm. Figure 5 shows that the overhang moment directly influences the open-loop gain G. Reductions in this moment reduce G with a consequential increase in stability, provided G is positive and has only a small imaginary part.

The test rotor exhibited a feature that did not occur during the production machine tests, merely because in the latter case the maximum speed was limited. The test rotor exhibited an upper limit above which stability was restored. The reason for this limit has been discussed in the theory; a sufficient but not exclusive condition for stability is that the real part of I_{OB} becomes positive, i.e., that the I_{OB} vector has a phase angle that increases through 270 deg with increasing speed. Figure 8 shows that such a condition exists at around 14,500 rpm, thus confirming the existence of an upper stability boundary. The exact speed at which this boundary occurs cannot be predicted from Fig. 8, but it must be less than 14,500 rpm. There is every reason to believe that the original compressor rotor too would have restabilized, if it had been possible to run at a high enough speed.

Conclusion

A vibration problem that could not directly be explained was encountered on a centrifugal compressor. A test rotor with dynamic characteristics identical to those of the compressor rotor has been built to verify a theory that could possibly explain the phenomenon. The experimental results obtained confirmed that differential heating of the bearing journals was the root cause of the unstable vibration behaviour. Even for a small orbit a significant temperature difference across the bearing journal was measured.

In particular, bearing thermal characteristics play an important role in thermal bending and a comprehensive program of theoretical and experimental research is being carried out in this field. The objective is to arrive at a bearing design, in which journal differential heating is minimized, while still retaining acceptable operating and dynamic characteristics.

Acknowledgments

The authors wish to thank Demag Delaval Turbomachinery for their permission to publish this paper.

References

1 ASME Power Test Codes "Compressors and Exhausters," PTC 10, 1965.
2 American Petroleum Institute standard "Centrifugal Compressors for General Refinery Service," API 617, 1979.
3 Newkirk, B. L., "Shaft Rubbing," *Mechanical Engineering,* Vol. 48, 1926, pp. 830–832.
4 Dimarogonas, A. D., "Newkirk Effect. Thermally Induced Dynamic Instability of High-Speed Rotors," ASME Paper No. 73-GT-26, 1973.
5 Kellenberger, W., "Spiral Vibrations Due to Seal Rings in Turbogenerators. Thermally Induced Interaction Between Rotor and Stator," ASME Paper No. 79-DET-61, 1979.
6 Schmied, J., "Spiral Vibrations of Rotors," *Rotating Machinery Dynamics,* Vol. 2, ASME, 1987.
7 Keogh, P. S., and Morton, P. G., "Journal Bearing Differential Heating Evaluation With Influence on Rotor Dynamic Behaviour," *Proceedings of the Royal Society, London,* Vol. A441, 1993, pp. 527–548.
8 Goodman, T. P., "A Least Squares Method for Computing Balance Corrections," ASME *Journal of Engineering for Industry,* Vol. 68, 1964, pp. 273–279.
9 Keogh, P. S., and Morton P. G., "The Dynamic Nature of Rotor Thermal Bending Due to Unsteady Lubricant Shearing Within a Bearing," *Proceedings of the Royal Society, London,* Vol. A445, 1994, pp. 273–290.

APPENDIX

Modeling Technique for Test Rotor

This appendix deals with a mathematical justification of the modeling technique for a reduced rotor length.

Any shaft can be modeled from a series of elements of diameter D_r, length L_r, and mass M_r. The bearing system can be

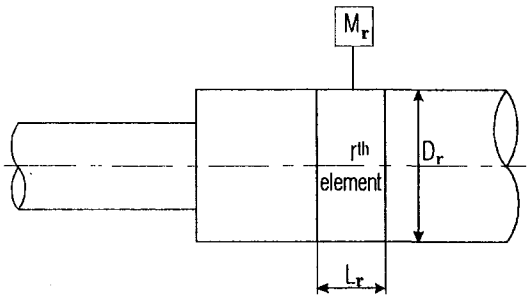

modeled as one set of notational stiffness and damping coefficients per bearing. Any "real" bearing needs four stiffness and four damping coefficients, and in the general case the shaft has to have degrees of freedom in both X and Y stationary axes.

The modeling technique can, however, be demonstrated more simply, but equally rigorously, by considering only vibrations in a single plane, with one stiffness and one damping coefficient per bearing. The homogeneous equations of motion for the system are expressed by the following matrix equation:

$$\left[\begin{array}{c|c} M & \\ \hline & k^2M \end{array}\right]\left[\begin{array}{c} \ddot{x} \\ \hline \ddot{\gamma} \end{array}\right] + \left[\begin{array}{c|c} C & \\ \hline & \end{array}\right]\left[\begin{array}{c} \dot{x} \\ \hline \dot{\gamma} \end{array}\right] + \left[\begin{array}{c|c} \dfrac{EI}{L^3}+K & \dfrac{EI}{L^2} \\ \hline \dfrac{EI}{L^2} & \dfrac{EI}{L} \end{array}\right]\left[\begin{array}{c} x \\ \hline \gamma \end{array}\right] = 0 \quad (8)$$

where:

- M is a diagonal submatrix with typical elements of mass $M + \rho\pi LD^2/4$
- k is the radius of gyration of each mass element
- C is a submatrix with two diagonal elements of bearing damping coefficients
- K comprises two diagonal elements of bearing stiffness coefficients
- E is the modulus of elasticity
- I is the moment of inertia
- EI/L^3 is the following submatrix:

$$\begin{bmatrix} \dfrac{12EI_1}{L_1^3} & \dfrac{-12EI_1}{L_1^3} & & \\ \dfrac{-12EI_1}{L_1^3} & \left(\dfrac{12EI_1}{L_1^3}+\dfrac{12EI_2}{L_2^3}\right) & \dfrac{-12EI_2}{L_2^3} & \\ & \dfrac{-12EI_2}{L_2^3} & \left(\dfrac{12EI_2}{L_2^3}+\dfrac{12EI_3}{L_3^3}\right) & \ddots \\ & & \ddots & \text{etc.} \end{bmatrix} \quad (9)$$

- EI/L^2 is the following submatrix:

$$\begin{bmatrix} \dfrac{6EI_1}{L_1^2} & \dfrac{6EI_1}{L_1^2} & & \\ \dfrac{6EI_1}{L_1^2} & \left(\dfrac{6EI_1}{L_1^2}+\dfrac{6EI_2}{L_2^2}\right) & \dfrac{6EI_2}{L_2^2} & \\ & \dfrac{6EI_2}{L_2^2} & \left(\dfrac{6EI_2}{L_2^2}+\dfrac{6EI_3}{L_3^2}\right) & \ddots \\ & & \ddots & \text{etc.} \end{bmatrix} \quad (10)$$

- EI/L is the following submatrix:

$$\begin{bmatrix} \dfrac{4EI_1}{L_1} & \dfrac{2EI_1}{L_1} & & \\ \dfrac{2EI_1}{L_1} & \left(\dfrac{4EI_1}{L_1}+\dfrac{4EI_2}{L_2}\right) & \dfrac{2EI_2}{L_2} & \\ & \dfrac{2EI_2}{L_2} & \left(\dfrac{4EI_2}{L_2}+\dfrac{4EI_3}{L_3}\right) & \ddots \\ & & \ddots & \text{etc.} \end{bmatrix} \quad (11)$$

We will now reduce the length of each rotor element by n (<1) and I by n^3. We will also reduce the radius of gyration k by $n^{1/2}$.

Consider the original shorthand form of the dynamic Eq. (8) for the full-scale rotor-bearing system. Now write a new set of equations for the model thus:

$$\left[\begin{array}{c|c} M & \\ \hline & Mk'^2 \end{array}\right]\left[\begin{array}{c} \ddot{x} \\ \hline \ddot{\eta} \end{array}\right] + \left[\begin{array}{c|c} C & \\ \hline & \end{array}\right]\left[\begin{array}{c} \dot{x} \\ \hline \dot{\eta} \end{array}\right] + \left[\begin{array}{c|c} \dfrac{EI'}{L'^3}+K & \dfrac{EI'}{L'^2} \\ \hline \dfrac{EI'}{L'^2} & \dfrac{EI'}{L'} \end{array}\right]\left[\begin{array}{c} x \\ \hline \eta \end{array}\right] = 0 \quad (12)$$

Substitute:

$$\eta = \gamma/n$$

$$k' = n^{1/2}k$$

$$L' = nL$$

$$I' = n^3I \quad \text{or} \quad D' = n^{3/4}D$$

The new equation now becomes:

$$\left[\begin{array}{c|c} M & \\ \hline & nk^2M \end{array}\right]\left[\begin{array}{c} \ddot{x} \\ \hline \ddot{\gamma} \end{array}\right] + \left[\begin{array}{c|c} C & \\ \hline & \end{array}\right]\left[\begin{array}{c} \dot{x} \\ \hline \dot{\gamma} \end{array}\right] + \left[\begin{array}{c|c} \dfrac{EI}{L^3}+K & \dfrac{EI}{L^2} \\ \hline \dfrac{EIn}{L^2} & \dfrac{EIn}{L} \end{array}\right]\left[\begin{array}{c} x \\ \hline \gamma \end{array}\right] = 0 \quad (13)$$

If we divide the lower equations throughout by n then the original form of Eq. (8) is obtained. This proves that the model is valid. However, it is inevitable that all shaft slopes will be increased by a factor $1/n$ because of the shortening of the rotor. This is not consequential.

In summary the diameter of shaft sections has to be reduced by the factor $n^{3/4}$ and the length by n. In order to achieve the same mass, the existing disk masses have to be increased to allow for the reduced shaft sections. Where there are no existing disks, these have to be added by shrinking onto the shaft. The shrink length of the added mass disks has to be kept small to avoid appreciable shaft stiffening. The diameter of the disks has to be adjusted to retain the same mass moment of inertia. It is necessary to maintain the geometry of the bearing journals.

This model neglects the effect of shear deflection in the scaling process, in the interests of geometric simplicity. To obtain the correct shear stiffness with a simple cylindrical element requires a diametral reduction of $n^{1/2}$, which is inconsistent with the scaling strategy adopted for bending. This is not an important consideration in a slender rotor.